ACS Photonics

pubs.acs.org/journal/apchd5
Article

Coupling-Controlled Photonic Topological Ring Array

Published as a part of the ACS Photonics special issue "Rising Stars in Photonics".

Chang Chang,[⊥] Yuhan Sun,[⊥] Ting Li, Binbin Weng,* and Yi Zou*

Cite This: https://doi.org/10.1021/acsphotonics.4c01502
Read Online

ABSTRACT: Photonic topological insulators with boundary states present a robust solution to mitigate structure imperfections. By alteration of the virtual boundary between trivial and topological insulators, it is possible to bypass such defects. Coupled resonator optical waveguides (CROWs) have demonstrated their utility in realizing photonic topological insulators, as they exhibit distinct topological phases and band structures. With this characteristic, we designed and experimentally validated a CROW array capable of altering its topological phase by adjusting the coupling strength. This array functions partially as a topological insulator and partially as a topologically trivial array, guiding light along the virtuous boundary between these two regions. By altering the shape of the topological insulator, we can effectively control the optical path. This approach promises practical applications, such as optical switches, dynamic light steering, optical sensing, and optical computing.

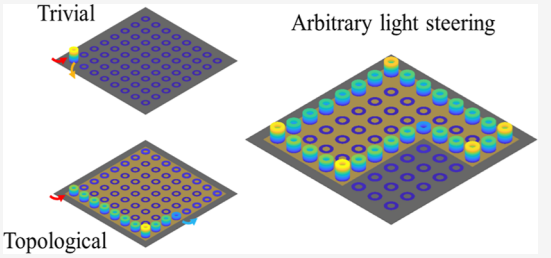

KEYWORDS: *topological photonics, anomalous floquet insulator, boundary state, light steering, waveguide*

INTRODUCTION

Integrated photonics has emerged as a versatile platform for exploring advanced physics and enabling a wide range of applications. However, the pursuit of higher performance has pushed fabrication techniques to their limits, making devices increasingly sensitive to imperfection. This issue is particularly pronounced in large-scale photonic integration, where the likelihood of fabrication errors escalates. While previous studies have focused on improving fabrication tolerance through carefully designed Mach−Zehnder interferometers and multimode ring resonators,[1,2] topological systems offer a novel approach to handling these imperfections.[3−5]

Periodic structures, known for their energy bands,[6−9] have found extensive applications across various fields.[10−15] Photonic topological insulators, a specialized class of these structures, are characterized by in-gap states localized at their boundaries.[16] Compared to nontopological methods, topological systems require stronger symmetry and exhibit greater robustness against disorder and defects. The topological state, protected by symmetry, is inherently more resistant to fabrication imperfections.[17,18] These insulators exhibit exotic boundary states that allow for arbitrary light steering through manipulation of virtue boundaries. Numerous theoretical[19−22] and experimental[23−27] approaches have been investigated for realizing photonic topological insulators. Some approaches utilize photonic crystal structures to introduce unique topological phases,[28−30] through these often involve units too small for precise individual control. Waveguide arrays,[31] while being powerful due to their inherent translational symmetry, are limited to one-dimensional periodicity, making on-chip two-dimensional light steering challenging. In contrast, optical ring arrays, also known as two-dimensional (2D) coupled resonator optical waveguides (CROWs), offer significant advantages. These include superior light confinement and precise phase control as light circulates within waveguides, and phase can be independently altered in individual rings. These properties are essential for reconfigurable devices in next-generation integrated systems.

Topological insulators based on CROW lattices have been effectively utilized in various applications, such as nonlinear conversion,[32] sensing,[33] light delay lines,[18,23] lasers,[34] and light steering.[25,35] Some approaches employ periodically varied coupling phases to emulate the magnetic field in quantum Hall systems,[23] while others use loss and gain mechanisms to achieve topological insulation.[25] Recent advancements have demonstrated programmable topological ring arrays through precise phase control at every lattice point.[36] However, the potential of combining topological insulators with trivial insulators remains largely untapped. CROW arrays hold considerable promise for integrated devices, particularly with further exploration of phase and coupling strength control. A special type of CROW array features identical site rings at each lattice point and identical link rings connecting these sites.

Received: August 8, 2024
Revised: November 8, 2024
Accepted: November 12, 2024

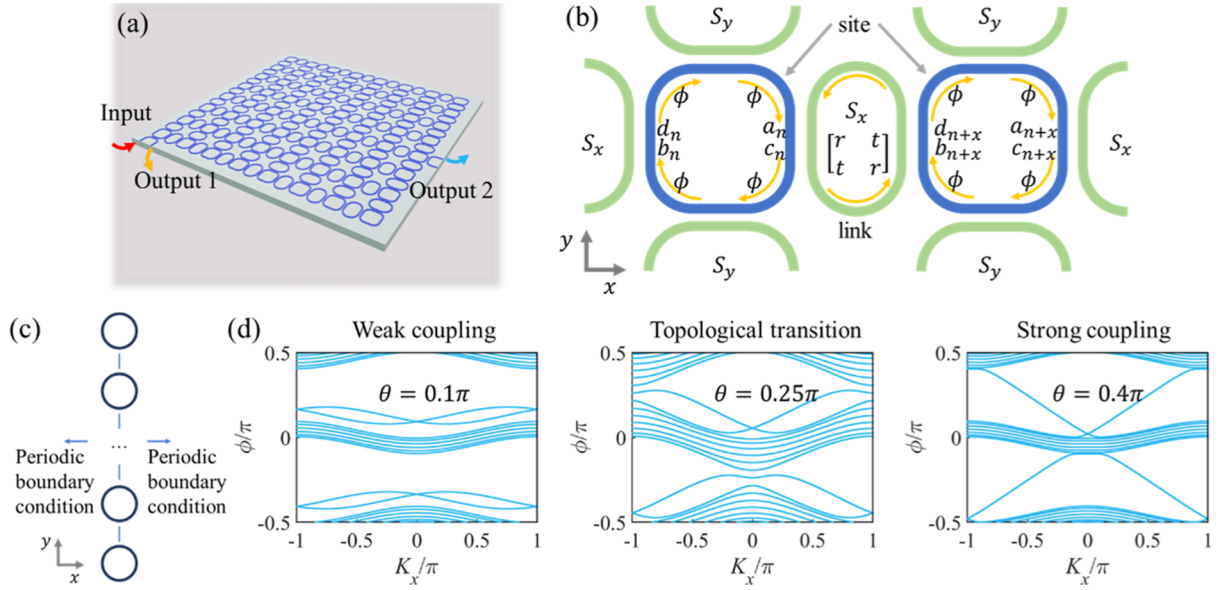

Figure 1. (a) Schematic of an 8 × 8 CROW lattice with input and output ports. (b) Schematic of two cells. Coupling between two lattices is represented by the coupling matrix S_x for the x-direction and S_y for the y-direction. Light traveling through a quarter of a site ring experiences a phase accumulation of ϕ. (c) Boundary condition used to derive the projected band diagram. (d) Projected band diagram showing the topological transition as the coupling between two lattices is tuned from weak to strong. The band gap closes and reopens during the transition, with edge states appearing.

Known as anomalous Floquet topological insulators (AFIs),[37] these structures require no additional loss or gain. AFIs, which possess zero Chern numbers due to time-reversal symmetry,[38] exhibit different topological phases under varying coupling strengths.[19,39] This property facilitates the redefinition of topological light pathways as the coupling in a ring resonator can be easily adjusted. By redefining the topological insulator area, the virtue boundary and boundary state can be modified, allowing light to follow any desired path within the CROW array's footprint. The 2D periodic symmetry of the CROW array permits expansion to any size, enabling light steering from any starting point to an arbitrary destination. These features position CROW arrays as an excellent solution for compact on-chip light steering.

In this letter, we design a CROW array capable of altering its topological phase under different intersite coupling strengths. Experimentally, we fabricated such a CROW array with an initial trivial insulator configuration. By applying a photoresist to enhance coupling, the CROW array transitions to a topological insulator with observable edge states. Both the output spectrum and the near-infrared (NIR) camera images confirm the presence of edge states and the topological phase transition from trivial to nontrivial. Our device operates across multiple wavelengths and occupies a footprint of only 350 × 350 μm^2. To demonstrate light steering capabilities, we created a virtue boundary with a topologically trivial bulk on one side and a topologically nontrivial bulk on the other, guiding light around the nontrivial area. This method fully leverages the footprint of a topological CROW array, which can be scaled and equipped with additional ports to achieve more complex functionalities.

RESULTS AND DISCUSSION

Our device consists of periodically arranged optical rings (Figure 1a). Each site in the array features a ring resonator positioned in a square lattice, coupled to neighboring rings via a link ring (Figure 1b). All site rings are identical, while the link rings share the same shape but have different orientations. For simplicity, we assume no spin mixing, meaning the clockwise circulating modes do not couple with the anticlockwise circulating modes. The lattice is described by a network model,[39] solvable by Bloch theory, with the phase accumulation ϕ through each quarter of a lattice ring serving as a quasi-energy.[38] Each lattice coordinate is denoted as $n = (x_n, y_n)$, where $n + x$ and $n + y$ represent the adjacent site units in the $+\hat{x}$ and $+\hat{y}$ directions, respectively. The coupling coefficient between link rings and site rings is given as κ. Combining these parameters with the phase accumulation through each half of a link ring φ, the coupling between adjacent sites can be specified by the complex numbers r, r', t, and t'. Given the symmetry and uniformity of the link rings in both directions, we have $r' = r$ and $t' = t$. In each lattice ring, we define four complex numbers a_n, b_n, c_n, and d_n to represent the amplitude at the input and output of the coupling region (Figure 1b). The coupling on two site rings can be expressed as

$$S_x \begin{bmatrix} a_n \\ b_{n+x} \end{bmatrix} = \begin{bmatrix} d_{n+x} \\ c_n \end{bmatrix} \tag{1}$$

$$S_y \begin{bmatrix} d_n \\ c_{n+y} \end{bmatrix} = \begin{bmatrix} b_{n+y} \\ a_n \end{bmatrix} e^{-2i\phi} \tag{2}$$

here

$$S_x = S_y = \begin{bmatrix} r & t \\ t & r \end{bmatrix} \tag{3}$$

Under the energy conservation law, the parameters can be defined according to coupled wave theory

$$r = \sin\theta,\ t = \cos\theta e^{i(\pm\pi/2)} \tag{4}$$

https://doi.org/10.1021/acsphotonics.4c01502
ACS Photonics XXXX, XXX, XXX−XXX

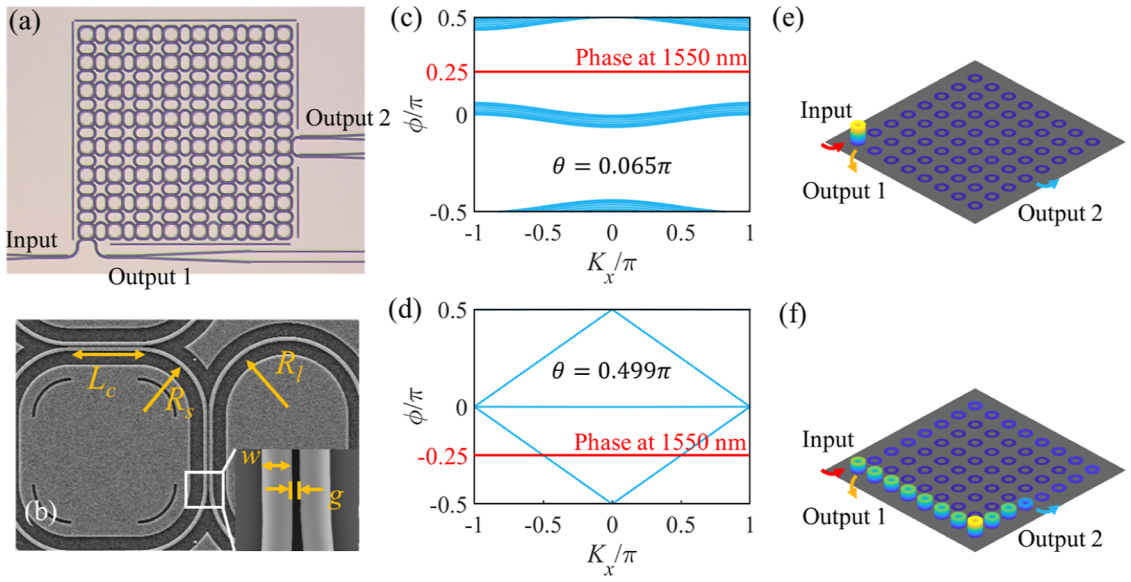

Figure 2. (a) Microscopic image of a fabricated 8 × 8 CROW array. (b) Zoom-in scanning electron microscopy image showing the key parameters of our device. The parameters are L_c = 8 μm, R_s = 7.998 μm, R_l = 9.010 μm, w = 480 nm, and g = 120 nm. (c) Band structure for the trivial insulator ($\theta = 0.065\pi$). There is no edge state in the band gap. At a wavelength of 1550 nm (red line), no mode exists that can propagate through the lattice. (d) Band structure for the topological insulator ($\theta = 0.499\pi$). A topological state appears in the gap. At a wavelength of 1550 nm (red line), light couples to the topological edge state. (e) Simulated field distribution under the topologically trivial condition, showing that light fails to enter the array as no state exists. (f) Simulated field distribution under the topologically nontrivial condition, showing light propagating around the array.

where $\theta \in [0,\pi/2]$ indicates the coupling strength. The phase sign in t depends on φ.

Using this formalism, we apply the Bloch theory to determine the dispersion relation between the Bloch wave vector and quasi-energy ϕ. The Bloch theory solutions take the form

$$a_{n+x} = e^{iK_x}a_n,\ a_{n+y} = e^{iK_y}a_n \tag{5}$$

where K_x and K_y are the Bloch wave vectors in the x and y directions, respectively. Note that b_n, c_n, and d_n have the same form. Applying periodic conditions in both directions results in no boundary states in the band diagram. To observe the topological phase change, we project the band to the x direction by calculating the dispersion relation of a semi-infinite strip with 8 site rings in the y direction and an infinite number in the x direction (Figure 1c). The results (Figure 1d) show that by tuning the coupling strength θ between site rings, a topological phase transition occurs. For weak couplings (θ = 0.1π), the band structure is gapped, the gap closes at a critical value (θ = 0.25π), and for strong couplings (θ = 0.4π), the gaps reopen with edge states spanning the band gaps.

In practice, the coupling θ can be adjusted by modifying the link ring and the phase accumulation ϕ by tuning the site ring.

Before detailing the device design, it is important to note that our device differs from topological insulators relying on synthetic magnetic vector potentials generated by periodically varying coupling.[23,39] In a tight-binding model, since coupling to other rings is very weak, one site ring is represented by one complex variable, whereas our network model assigns two independent complex variables a_n and b_n to each site ring due to stronger coupling. This distinction is crucial in the strong coupling CROW array, as strong coupling precludes treating the four-quarters of one site ring as identical.

Based on the aforementioned theory, we designed and fabricated a device on a silicon-on-insulator (SOI) wafer. The top view of a fabricated 8 × 8 array and key parameters are shown in Figure 2a,b. As described, the array includes site and link rings with scattering structures at each corner of the site rings to facilitate camera imaging. The straight lines outside the resonator array are used as a centering mark in camera view. The device operates at a wavelength of 1550 nm, which is common in optical communication. The waveguide dimensions are set to 480 nm in width and 220 nm in height to ensure single-mode propagation and acceptable loss. The first design step involves creating a directional coupler between the site and link rings, with coupling strength κ significantly impacting intersite coupling. Simulations indicate that a 120 nm gap and an 8 μm length L_c are appropriate, allowing for photoresist application to alter coupling strength and achieving a substantial coupling coefficient κ when the photoresist is applied. The turning radius of the link ring is adjusted to ensure, for the targeting wavelength, i.e., 1550 nm, the strongest intersite coupling with photoresist and the weakest with air cladding. The optimal radius R_l is determined to be 9.010 μm, balancing phase certainty and minimizing additional loss.

Projected band diagrams for weak coupling (θ = 0.065π) and strong coupling (θ = 0.499π) are shown in Figure 2c,d. The site ring radius R_s is set to 7.998 μm to position ϕ at the middle of the gap in both scenarios (red lines in Figure 2c,d). Experimentally, slight deviations in wavelength shift both ϕ and the entire band, so the working wavelength is centered in the gap to ensure device functionality despite design variations.

Under weak coupling, the CROW array acts as a trivial insulator, preventing light from entering the bulk or boundary (Figure 2e). Under strong coupling, while the bulk remains an insulator, light can instead effectively couple to the topological edge states (Figure 2f). This phenomenon is demonstrated by injecting light to one site ring on the edge and observing the intensity distribution at each site ring. We experimentally verify our design using a finite 8 × 8 array. In our experiments, we demonstrate that the CROW array functions as a trivial

https://doi.org/10.1021/acsphotonics.4c01502
ACS Photonics XXXX, XXX, XXX−XXX

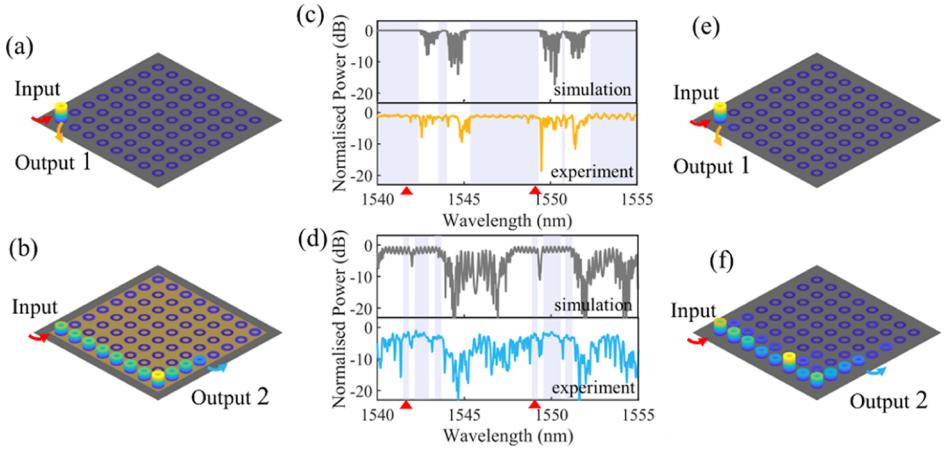

Figure 3. Schematic of an 8 × 8 CROW lattice with input and output ports, with simulated intensity represented by height. The device functions as (a) trivial insulator before applying photoresist and (b) topological insulator after applying photoresist. Simulated and measured transmission spectra of the CROW lattice (c) from output 1 for a trivial insulator and (d) from output 2 for a topological insulator. Red arrows indicate the wavelengths that simultaneously achieve the trivial insulator and topological insulator states. Maps of scattered light intensity constructed from NIR camera data for (e) trivial insulator and (f) topological insulator.

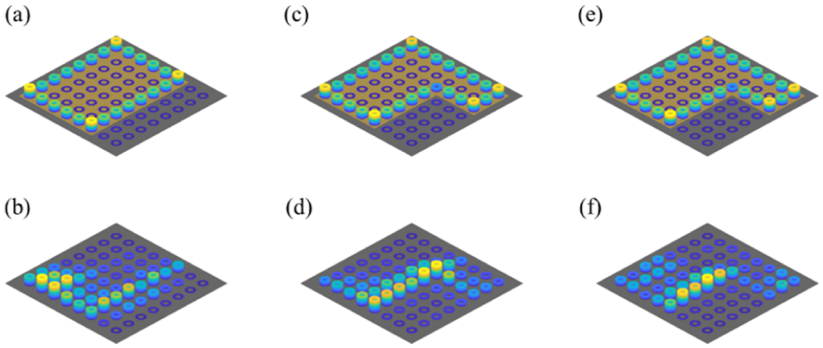

Figure 4. (a) Simulated intensity distribution at a wavelength of 1549 nm. The yellow area indicates the photoresist cladding. (b) Mapped intensity distribution of the fabricated device at 1549 nm. (c) Simulated intensity distribution at a wavelength of 1549 nm with an L-shaped photoresist cladding pattern. (d) Mapped intensity distribution of the fabricated device with L-shaped photoresist cladding at 1549 nm. (e) Simulated intensity distribution at a wavelength of 1541.8 nm with an L-shaped photoresist cladding pattern. (f) Mapped intensity distribution of the fabricated device with L-shaped photoresist cladding at 1541.8 nm.

insulator under air cladding and as a topological insulator under photoresist (AZ5214 with refractive index of 1.60) cladding, as shown in Figure 3a,b. The device features one input and two outputs, labeled outputs 1 and 2. For the topologically trivial insulator, we excite the structure through the input port. When in the band gap, we expect high transmission from input to output 1, as the bulk is insulating. The normalized transmission spectrum from the input to output 1 is shown in Figure 3c over the 1540−1555 nm wavelength range. We included the simulated spectrum for comparison. Several band gaps (gray regions) exhibit high power transmission to Output 1, where light cannot couple to a bulk state and therefore does not propagate through the lattice. Although the fabricated device's transmission band shifts due to deviations in the link ring and site ring phases (detailed in Supplementary Note S1 Section 3), the overall spectral behavior remains similar. Therefore, we present the simulated spectrum corresponding to the fabricated device's phase.

For the topological insulator, we used the same input port. This time, light couples to the topological edge state and reaches output 2, resulting in high transmission from the input to output 2. The simulated and experimental transmission results for output 2 are shown in Figure 3d. Several band gaps (gray regions) exhibit high power transmission from the input to output 2, where the bulk remains insulating, but light propagates as an edge mode. At some wavelengths outside the gray regions, edge states still exist because the high transmission band in the simulation is broader than the measured spectrum. This discrepancy is due to some directional coupler not being fully infiltrated by the photoresist, causing resonance peaks in the spectrum. Light paths at different wavelengths are observed using a NIR camera (see Supplementary Video S1).

To achieve both trivial and topological insulator states at the same wavelength, we set the working wavelengths to 1549 and 1541.8 nm, as indicated by the red arrows in Figure 3c,d. At these wavelengths, we achieve a topological insulator with air cladding and a trivial insulator with photoresist cladding. To obtain direct evidence of AFI edge modes in the bulk band gaps, we inject light at a wavelength of 1549 nm, which lies within the band gap, into the input waveguide and image the scattered light pattern using an NIR camera. Light intensity distributions for both scenarios are shown in Figure 3e,f. The intensity captured by the camera is based on scattered light, displaying random-like properties, and is not directly propor-

https://doi.org/10.1021/acsphotonics.4c01502
ACS Photonics XXXX, XXX, XXX−XXX

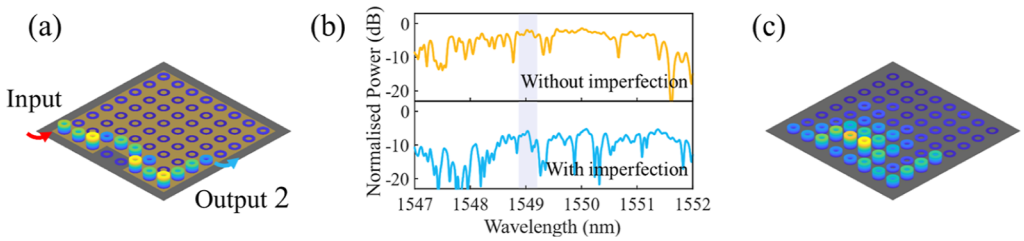

Figure 5. (a) Schematic of an 8 × 8 CROW lattice with a twisted virtue boundary, with intensity represented by height. (b) Transmission spectrum comparison with and without a detour. (c) Mapped intensity distribution of the fabricated device with a twisted photoresist cladding boundary at 1549 nm.

tional to the light intensity in the waveguide. When the wavelength lies within the bulk band, bulk states are excited (Supplementary Video S2).

By covering part of the device with different photoresist patterns, we demonstrate light propagation through a synthetic interface. We tested the device at wavelengths of 1549 and 1541.8 nm, where it simultaneously acted as a topological and trivial insulator. Simulated results showing light intensity distribution at 1549 nm with square and L-shaped topological insulators are presented in Figure 4a,c, and at 1541.8 nm in Figure 4e. These simulations are consistent with the theory. Experimental results of the mapped intensity distribution are shown in Figure 4b,d,f. Exciting the input port at the edge of the topologically nontrivial domain, the images captured by the NIR camera verify the light steering capability of our device.

To verify the robustness of the topological edge state, we introduce fabrication errors at the boundary through leaving two sites and two ling rings with air cladding and adjusted the virtual boundary to bypass these errors. As shown in the simulation result in Figure 5a, we model a fabrication error at the device boundary and move the virtual boundary to create a detour. The spectrum indicated a transmission drop of about 4 dB at 1549 nm due to this detour, as shown in Figure 5b. We note that such a boundary would introduce backscattering, causing coupling between two pseudospins.[19] The abrupt change in cladding index and scattering at the edge of the photoresist-covered area affect the transmission spectrum. Other coupling tuning methods, such as electro-optic the phase shifter on the link ring, could address this issue (see Supplementary Note S5). Despite this, the topological protection ensured that the edge state could circumvent the trivial insulator part and continue propagating along the modified edge (Figure 5c). Although this defect impacts the one-way propagation behavior of the edge state, the CROW lattice retains its topological nature. We discuss additional fabrication error scenarios in Supplementary Note S4.

CONCLUSIONS

In conclusion, we design and experimentally demonstrate a Floquet TPI whose topological phase can be tuned by adjusting the coupling strength. The lattice with air cladding functions as a trivial insulator, preventing any states in the band gap, while the lattice with photoresist cladding acts as a higher refractive index, promoting a nontrivial topological insulator with edge states in the band gap. By creating a synthetic interface between the topological and trivial insulators, we achieve an effective light steering. Additionally, we verified the robustness of the topological edge state by introducing detours at the boundary. To further reduce the device footprint, the coupler can be replaced with a more compact structure.[40] The intersite coupling strength can be adjusted by various methods beyond the application of photoresist, such as utilizing phase shifters on the link ring via carrier dispersion effects[41,42] or electro-optic effects.[43,44] This adaptability could allow the CROW array to serve as an optical switch, router, and sensors. Our work, therefore, provides a novel engineering pathway for robust routing and switching of light in integrated photonic circuits.

ASSOCIATED CONTENT

Data Availability Statement

The data that support the findings of this study are available from the corresponding author upon reasonable request.

Supporting Information

The Supporting Information is available free of charge at https://pubs.acs.org/doi/10.1021/acsphotonics.4c01502.

Fabrication, experiment setup, deviation from design, influence of fabrication imperfection, effect of boundary phase, comment on other possible tuning methods, and comparison with regular photonic circuits (PDF)

Camera image of the topological state (AVI)

Camera image of the trivial state (AVI)

AUTHOR INFORMATION

Corresponding Authors

Binbin Weng − *School of Electrical and Computer Engineering, University of Oklahoma, Norman, Oklahoma 73019, United States*; Email: binbinweng@ou.edu

Yi Zou − *School of Information Science and Technology, ShanghaiTech University, Shanghai 201210, China*; orcid.org/0000-0002-7675-8542; Email: zouyi@shanghaitech.edu.cn

Authors

Chang Chang − *School of Information Science and Technology, ShanghaiTech University, Shanghai 201210, China; Chinese Academy of Sciences, Shanghai Institute of Microsystem & Information Technology, Shanghai 200050, China; University of Chinese Academy of Sciences, Beijing 100049, China*; orcid.org/0009-0007-8823-212X

Yuhan Sun − *School of Information Science and Technology, ShanghaiTech University, Shanghai 201210, China; Chinese Academy of Sciences, Shanghai Institute of Microsystem & Information Technology, Shanghai 200050, China; University of Chinese Academy of Sciences, Beijing 100049, China*; orcid.org/0000-0003-0184-2325

Ting Li − *School of Information Science and Technology, ShanghaiTech University, Shanghai 201210, China*; orcid.org/0009-0004-9156-3630

https://doi.org/10.1021/acsphotonics.4c01502
ACS Photonics XXXX, XXX, XXX−XXX

Complete contact information is available at:
https://pubs.acs.org/10.1021/acsphotonics.4c01502

Author Contributions

[⊥]C. C. and Y. S. contributed equally to this paper.C. C., B. W., and Y. Z. conceived the idea. C. C. proposed the design and performed the numerical simulations; Y. S. fabricated the samples; C. C., performed the measurements; C. C., Y. S., and T. L. analyzed the results; and C. C. wrote the manuscript with the input from all authors. B. W. provides advisory support in preparing the manuscript. Y. Z. supervised the project, provided experimental funding support, and polished the manuscript.

Funding

The research was sponsored by the Natural Science Foundation of Shanghai (21ZR1443100). B. W. acknowledges a partial support from the U.S. National Science Foundation Early Career program (2340060).

Notes

The authors declare no competing financial interest.

■ ACKNOWLEDGMENTS

The authors thank the ShanghaiTech Material and Device Lab (SMDL) for technique support.

■ REFERENCES

(1) Papadovasilakis, M.; Chandran, S.; Gebregiorgis, Y.; Bian, Y.; Rakowski, M.; Krishnamurthy, S.; Aboketaf, A.; Augur, R.; Viegas, J. Fabrication tolerant and wavelength independent arbitrary power splitters on a monolithic silicon photonics platform. *Opt. Express* **2022**, *30* (19), 33780−33791.
(2) Netherton, A. M.; Gao, Y.; Pestana, N.; Bovington, J.; Bowers, J. E. Athermal fabrication-tolerant Si-SiN FIR filters for a silicon photonics foundry platform. *Opt. Express* **2023**, *31* (15), 23952−23965.
(3) Lu, L.; Joannopoulos, J. D.; Soljačić, M. Topological photonics. *Nat. Photonics* **2014**, *8* (11), 821−829.
(4) Zhang, Z.; Delplace, P.; Fleury, R. Superior robustness of anomalous non-reciprocal topological edge states. *Nature* **2021**, *598* (7880), 293−297.
(5) Hasan, M. Z.; Kane, C. L. Colloquium: Topological insulators. *Rev. Mod. Phys.* **2010**, *82* (4), 3045−3067.
(6) He, W.; Sun, Y.; Zhou, P.; Xia, L.; Li, T.; Yi, Q.; Shen, L.; Cheng, Z.; Zou, Y. Subwavelength structure engineered passband filter for the 2-μm wave band. *Opt. Lett.* **2023**, *48* (3), 827−830.
(7) Tang, S.; Chang, C.; Zhou, P.; Zou, Y. Numerical Study on a Bound State in the Continuum Assisted Plasmonic Refractive Index Sensor. *Photonics* **2022**, *9* (4), 224.
(8) Zou, Y.; Chakravarty, S.; Chen, R. T. Mid-infrared silicon-on-sapphire waveguide coupled photonic crystal microcavities. *Appl. Phys. Lett.* **2015**, *107* (8), 081109.
(9) Zou, Y.; Chakravarty, S.; Zhu, L.; Chen, R. T. The role of group index engineering in series-connected photonic crystal microcavities for high density sensor microarrays. *Appl. Phys. Lett.* **2014**, *104* (14), 141103.
(10) Zhou, P.; Li, T.; Lin, Y.; Xia, L.; Shen, L.; Xu, X.; Li, T.; Zou, Y. Artificial Gauge Field Enabled Low-Crosstalk, Broadband, Half-Wavelength Pitched Waveguide Arrays. *Laser Photonics Rev.* **2023**, *17* (6), 2200944.
(11) Hu, Y.; He, W.; Sun, Y.; Yi, Q.; Xing, S.; Yan, Z.; Xia, L.; Li, T.; Zhou, P.; Zhang, J.; Shen, L.; Zou, Y. High-efficient subwavelength structure engineered grating couplers for 2-μm waveband high-speed data transmission. *Opt. Express* **2023**, *31* (23), 39079−39087.
(12) Liu, Y.; Xia, L.; Li, T.; Sun, Y.; Zhou, P.; Shen, L.; Zou, Y. High-efficiency mid-infrared on-chip silicon grating couplers for perfectly vertical coupling. *Opt. Lett.* **2023**, *48* (2), 239−242.
(13) Sun, Y.; Li, T.; Zhou, P.; Zou, Y. Subwavelength-Structured High-Efficiency Nanophotonic Coupler for Air Top-Cladded Silicon Waveguide. *IEEE Photonics J.* **2021**, *13* (4), 1−5.
(14) Xiao, Z.; Liu, W.; Xu, S.; Zhou, J.; Ren, Z.; Lee, C. Recent Progress in Silicon-Based Photonic Integrated Circuits and Emerging Applications. *Adv. Opt. Mater.* **2023**, *11* (20), 2301028.
(15) Sun, F.; Dong, B.; Wei, J.; Ma, Y.; Tian, H.; Lee, C. Demonstration of mid-infrared slow light one-dimensional photonic crystal ring resonator with high-order photonic bandgap. *Opt. Express* **2020**, *28* (21), 30736−30747.
(16) Tang, G. J.; He, X. T.; Shi, F. L.; Liu, J. W.; Chen, X. D.; Dong, J. W. Topological Photonic Crystals: Physics, Designs, and Applications. *Laser Photonics Rev.* **2022**, *16* (4), 31.
(17) Leykam, D.; Yuan, L. Topological phases in ring resonators: recent progress and future prospects. *Nanophotonics* **2020**, *9* (15), 4473−4487.
(18) Mittal, S.; Fan, J.; Faez, S.; Migdall, A.; Taylor, J. M.; Hafezi, M. Topologically Robust Transport of Photons in a Synthetic Gauge Field. *Phys. Rev. Lett.* **2014**, *113* (8), 087403.
(19) Liang, G. Q.; Chong, Y. D. Optical Resonator Analog of a Two-Dimensional Topological Insulator. *Phys. Rev. Lett.* **2013**, *110* (20), 203904.
(20) Raghu, S.; Haldane, F. D. M. Analogs of quantum-Hall-effect edge states in photonic crystals. *Phys. Rev. A* **2008**, *78* (3), 033834.
(21) Fang, K.; Yu, Z.; Fan, S. Realizing effective magnetic field for photons by controlling the phase of dynamic modulation. *Nat. Photonics* **2012**, *6* (11), 782−787.
(22) Smirnova, D. A.; Smirnov, L. A.; Leykam, D.; Kivshar, Y. S. Topological Edge States and Gap Solitons in the Nonlinear Dirac Model. *Laser Photonics Rev.* **2019**, *13* (12), 1900223.
(23) Hafezi, M.; Mittal, S.; Fan, J.; Migdall, A.; Taylor, J. M. Imaging topological edge states in silicon photonics. *Nat. Photonics* **2013**, *7* (12), 1001−1005.
(24) Wang, H.; Tang, G.; He, Y.; Wang, Z.; Li, X.; Sun, L.; Zhang, Y.; Yuan, L.; Dong, J.; Su, Y. Ultracompact topological photonic switch based on valley-vortex-enhanced high-efficiency phase shift. *Light: Sci. Appl.* **2022**, *11* (1), 292.
(25) Zhao, H.; Qiao, X.; Wu, T.; Midya, B.; Longhi, S.; Feng, L. Non-Hermitian topological light steering. *Science* **2019**, *365* (6458), 1163−1166.
(26) Kudyshev, Z. A.; Kildishev, A. V.; Boltasseva, A.; Shalaev, V. M. Tuning Topology of Photonic Systems with Transparent Conducting Oxides. *ACS Photonics* **2019**, *6* (8), 1922−1930.
(27) Zeng, Y.; Chattopadhyay, U.; Zhu, B.; Qiang, B.; Li, J.; Jin, Y.; Li, L.; Davies, A. G.; Linfield, E. H.; Zhang, B.; Chong, Y.; Wang, Q. J. Electrically pumped topological laser with valley edge modes. *Nature* **2020**, *578* (7794), 246−250.
(28) Wu, M.; Yang, Y.; Fei, H.; Lin, H.; Zhao, X.; Kang, L.; Xiao, L. On-Chip Ultra-Compact Hexagonal Boron Nitride Topological Ring-Resonator in Visible Region. *J. Lightwave Technol.* **2022**, *40* (23), 7610−7618.
(29) He, X.-T.; Liang, E.-T.; Yuan, J.-J.; Qiu, H.-Y.; Chen, X.-D.; Zhao, F.-L.; Dong, J.-W. A silicon-on-insulator slab for topological valley transport. *Nat. Commun.* **2019**, *10* (1), 872.
(30) You, J. W.; Ma, Q.; Lan, Z.; Xiao, Q.; Panoiu, N. C.; Cui, T. J. Reprogrammable plasmonic topological insulators with ultrafast control. *Nat. Commun.* **2021**, *12* (1), 5468.
(31) Song, W.; Wu, S.; Chen, C.; Chen, Y.; Huang, C.; Yuan, L.; Zhu, S.; Li, T. Observation of Weyl Interface States in Non-Hermitian Synthetic Photonic Systems. *Phys. Rev. Lett.* **2023**, *130* (4), 043803.
(32) Mittal, S.; Goldschmidt, E. A.; Hafezi, M. A topological source of quantum light. *Nature* **2018**, *561* (7724), 502−506.
(33) Arledge, K. E.; Uchoa, B.; Zou, Y.; Weng, B. Topological sensing with photonic arrays of resonant circular waveguides. *Phys. Rev. Res.* **2021**, *3* (3), 033106.
(34) Zhao, H.; Miao, P.; Teimourpour, M. H.; Malzard, S.; El-Ganainy, R.; Schomerus, H.; Feng, L. Topological hybrid silicon microlasers. *Nat. Commun.* **2018**, *9* (1), 981.

(35) Kudyshev, Z. A.; Kildishev, A. V.; Boltasseva, A.; Shalaev, V. M. Photonic topological phase transition on demand. *Nanophotonics* **2019**, *8* (8), 1349−1356.
(36) Dai, T.; Ma, A.; Mao, J.; Ao, Y.; Jia, X.; Zheng, Y.; Zhai, C.; Yang, Y.; Li, Z.; Tang, B.; Luo, J.; Zhang, B.; Hu, X.; Gong, Q.; Wang, J. A programmable topological photonic chip. *Nat. Mater.* **2024**, *23* (7), 928−936.
(37) Rudner, M. S.; Lindner, N. H.; Berg, E.; Levin, M. Anomalous Edge States and the Bulk-Edge Correspondence for Periodically Driven Two-Dimensional Systems. *Phys. Rev. X* **2013**, *3* (3), 031005.
(38) Pasek, M.; Chong, Y. D. Network models of photonic Floquet topological insulators. *Phys. Rev. B* **2014**, *89* (7), 075113.
(39) Gao, F.; Gao, Z.; Shi, X.; Yang, Z.; Lin, X.; Xu, H.; Joannopoulos, J. D.; Soljačić, M.; Chen, H.; Lu, L.; Chong, Y.; Zhang, B. Probing topological protection using a designer surface plasmon structure. *Nat. Commun.* **2016**, *7* (1), 11619.
(40) Zhang, A.; Xia, L.; Li, T.; Chang, C.; Zhou, P.; Xu, X.; Zou, Y. Ultra-compact polarization-independent 3 dB power splitter in silicon. *Opt. Lett.* **2021**, *46* (19), 5000−5003.
(41) Sun, J.; Kumar, R.; Sakib, M.; Driscoll, J. B.; Jayatilleka, H.; Rong, H. A 128 Gb/s PAM4 Silicon Microring Modulator with Integrated Thermo-Optic Resonance Tuning. *J. Lightwave Technol.* **2019**, *37* (1), 110−115.
(42) Thiessen, T.; Grosse, P.; Fonseca, J. D.; Billondeau, P.; Szelag, B.; Jany, C.; Poon, J. k. S.; Menezo, S. 30 GHz heterogeneously integrated capacitive InP-on-Si Mach-Zehnder modulators. *Opt. Express* **2019**, *27* (1), 102−109.
(43) Demkov, A. A.; Posadas, A. B. Ferroelectric BaTiO3 for Electro-Optic Modulators in Si Photonics. *IEEE J. Sel. Top. Quantum Electron.* **2024**, *30*, 3405387.
(44) Li, W.; Eltes, F.; Berikaa, E.; Alam, M. S.; Bernal, S.; Minkenberg, C.; Abel, S.; Plant, D. V. Thin-Film BTO-Based MZMs for Next-Generation IMDD Transceivers Beyond 200 Gbps/λ. *J. Lightwave Technol.* **2024**, *42* (3), 1143−1150.

https://doi.org/10.1021/acsphotonics.4c01502
ACS Photonics XXXX, XXX, XXX−XXX